Note: Snapshot PDF is the proof copy of corrections marked in EditGenie, the layout would be different from typeset PDF and EditGenie editing view.

## Author Queries & Comments:

**Q1 :** Please note that the ORCID has/have been created from information provided through CATS. Please correct if this is inaccurate.

Response: Resolved

**Q2 :** Funding details have been taken from information supplied with your manuscript submission. Please correct if this is inaccurate.

Response: Resolved. "Junta de Andalucía" was removed from this "Funding" section. This is mentioned in the "Acknowledgments" section.

**Q3 :** The funding information provided (National Agency for Scientific and Technological Promotion) has been checked against the Open Funder Registry and we failed to find a match. Please check and resupply the funding details.

Response: Resolved. The funding details were given.

**Q4 :** Please note that this Funding information "10.13039/501100011011Junta de Andalucía" has been created from information provided through CATS. Please correct if this is inaccurate.

Response: Resolved. "Junta de Andalucía" was removed from this section. This is mentioned in the "Acknowledgments" section.

**Q5 :** Please provide missing city for the reference "[b1]" references list entry.

Response: Resolved. The city was provided.

**Q6 :** Please provide missing city for the reference "[b2]" references list entry.

Response: Resolved. The city was provided.

**Q7 :** Please provide missing city for the reference "[b3]" references list entry.

Response: Resolved. The city was provided.

---

# Multi-isotope ($\delta^2$H, $\delta^{18}$O, $\delta^{13}$C-TDIC, $\delta^{18}$O-TDIC, $^{87}$Sr/$^{86}$Sr) and hydrochemical study on fractured-karstic and detritic shallow aquifers in the Pampean region, Argentina

**Recto running head :** ISOTOPES IN ENVIRONMENTAL AND HEALTH STUDIES

**Verso running head :** M. GLOK-GALLI ET AL.

Melisa Glok-Galli[a,b] **[Q1]**, Daniel E. Martínez[b,c], Iñaki Vadillo-Pérez[d], Adrián A. Silva Busso[e], Silvia P. Barredo[f], Orlando M. Quiroz Londoño[b,c], Mónica A. Trezza[a]

[a] Facultad de Ingeniería (UNCPBA)-CIFICEN (UNCPBA-CICPBA-CONICET), Olavarría, Argentina

[b] Grupo de Hidrogeología, IGCyC (UNMDP-CICPBA), Mar del Plata, Argentina

[c] Instituto de Investigaciones Marinas y Costeras (UNMDP-CONICET), Mar del Plata, Argentina

[d] Centro de Hidrogeología, Universidad de Málaga, Málaga, Spain

[e] Universidad de Buenos Aires (UBA), Buenos Aires, Argentina

[f] Grupo de Modelado Estático y Dinámico de Cuencas, IGPUBA, CABA, Buenos Aires, Argentina

**CONTACT** Melisa Glok-Galli glokgalli@mdp.edu.ar, melisaglokgalli@gmail.com

Supplemental data for this article can be accessed https://doi.org/10.1080/10256016.2020.1825412

**History :** received : 2020-03-13 accepted : 2020-08-14



**ABSTRACT**

Fluxes between fractured-karstified and detritic aquifers are commonly poorly understood in many environments. These two types of aquifers are in contact in the southeastern Pampean region in the Argentine Buenos Aires province, and the aim of this work is to analyze their relationship contributing to improve the hydrological model. A joint application of hydrochemical and multi-isotope ($\delta^2$H, $\delta^{18}$O, $\delta^{13}$C-TDIC, $\delta^{18}$O-TDIC, $^{87}$Sr/$^{86}$Sr) tools was used. TDIC, $\delta^2$H, $\delta^{18}$O and $\delta^{13}$C-TDIC allowed differentiating two main end members. Water in the Pampeano aquifer (PA) which is transferred from the fractured-karstic aquifer (F-KA) is characterised by high TDIC around 500–700 mg/L, isotopically depleted in $^{18}$O (about −5.5 ‰) and high $\delta^{13}$C-TDIC (around −10.0 ‰). The other end member is direct recharge water infiltrated into the PA with TDIC ranging from 400 to 500 mg/L, slightly enriched in $^{18}$O ($\delta^{18}$O = −4.8 ‰), and $\delta^{13}$C-TDIC in the range of soil $CO_2$ as a result of

reactions with calcrete concretions (from −20.0 to −9.0 ‰). Dolomite dissolution is the main process controlling the chemistry of the low-mineralized (Mg–Ca-$HCO_3$) waters, whereas high-mineralized (Na-$HCO_3$) waters are strongly influenced by ion-exchange reactions with adsorbed $Ca^{2+}$ and $Mg^{2+}$ and by evaporation.

**KEYWORDS**

- Argentine Pampean region
- carbon-13
- fractured-karstic aquifers
- hydrogen-2
- isotope hydrology
- oxygen-18
- Pampeano aquifer
- $^{87}Sr/^{86}Sr$
- TDIC

**FUNDING**

**[Q2]**The authors would like to thank the financial support of the "Agencia Nacional de Promoción Científica y Tecnológica" ~~ANPCyT~~ (National Agency for Scientific and Technological Promotion -ANPCyT-, Argentina) through PICT 2016 N°1625~~,~~ **[Q3]**~~Junta de Andalucía~~**[Q4]**.

## 1. Introduction

Low-permeability crystalline rocks that include heavily cemented igneous, metamorphic and sedimentary rocks are commonly considered as hydrological basement. Nevertheless, these can be affected by faults, joints, fractures or by their own weathering profile, allowing the circulation of significant amounts of water. Fractured geological formations are the most frequent in nature [1,2], and three quarters of the continents' global surface are dominated by fractured aquifers [3].

Carbonates are very abundant in the Earth's crust, representing about 5% in volume of the lithosphere and approximately 15% of the total sedimentary deposits [4], the latter being more susceptible to water attack than non-carbonated rocks. The dissolution process on carbonate rocks originates from a secondary porosity which leads to the formation of good quality aquifers, in a phenomenon known as karstification, creating karst aquifer systems [5–7]. Water transfer between the two systems can occur in areas where fractured-karstic aquifers (F-KAs) and detritic aquifers are in contact.

Fluxes among fractured-karstified and detritic aquifers are poorly understood in many environments, missing important information for a sustainable use of water resources. The interpretation of hydrochemical and isotopic signatures can be a useful tool in understanding recharge and mixing between aquifer systems [8–16]. In particular, the analysis of water stable isotopes ($\delta^2H$ and $\delta^{18}O$) in different hydrological components has a number of applications enabling the understanding of groundwater dynamics [17,18]. As with the infiltration rate, permeability and dispersivity in F-KAs and detritic aquifers are different, it is possible to expect differences in the isotopic fingerprint of water in some cases, mainly due to faster and preferred recharge in fractures, mixing in the non-saturated zone or local evaporation processes taking place during infiltration [19].

The carbon-13 of total dissolved inorganic carbon ($\delta^{13}C$-TDIC) is another environmental stable isotope with diverse applications in hydrological studies [17,18,20]. Dissolved inorganic carbon sources contributing to groundwater can be assessed using $\delta^{13}C$-TDIC. $^{18}O$ in its various dissolved carbonate phases ($CO_2$, $HCO_3^-$ and $CO_3^{2-}$) exchanges rapidly with water and therefore cannot be used to trace the origin of carbon. However, when calcite is precipitated from water, it preserves a record of the $\delta^{18}O$-TDIC of water; this is a powerful tool as it can record changes in water balances [17]. Strontium is a divalent cation that can replace calcium in minerals' structures. The $^{87}Sr/^{86}Sr$ ratio is as well a very useful indicator in hydrological systems, the analysis and interpretation of which can help to understand and to quantify mixing between different sources, whether natural or anthropogenic [21–24].

In Argentina, few hydrogeological studies have been conducted on fractured and karstic aquifers in areas such as the Precordillera [25,26]. In Buenos Aires province, southeastern Pampean region, a variety of crystalline rock outcrops is observed in the Tandilia Mountain System (TMS), a 350 km long, northwest–southeast oriented orographic belt. Its extension covers from Olavarría to the city of Mar del Plata (located ~ 300 km south from Olavarría city) [27–30]. The analysis of $\delta^2H$ and $\delta^{18}O$ indicates that water transfer possibly exists between the fractured aquifer and the detritic aquifer (Pampeano aquifer, PA) in the southern end of the TMS [19].

The Olavarría Mountain Ranges is one of the groups in which the TMS is divided and where the study area is located (Figure 1). While the F-KAs are not currently exploited in this zone, the host rocks are subject to important mining extraction. The PA is the water supply source for urban, agricultural and industrial use. In this area, more accurately in the Tapalqué Creek Upper Basin (TCUB), Auge [31], Díaz et al. [32,33], Kruse et al. [34], Varela [35] and Varela et al. [36] undertook climatological, hydrogeological and hydrogeochemical studies of surface water (SW) and groundwater of the PA, obtaining the former piezometric map of the catchment area, evidencing the gaining behaviour of the TCUB streams. Glok-Galli et al. [37,38] added the $\delta^2H$ and $\delta^{18}O$ characterisation of these types of waters to these studies, updated the piezometric map of the basin, and corroborated the predominance of the PA discharge into SW body flow.

**Figure 1.** Location map (DEM (m a.s.l.): Digital Elevation Model (meters above sea level), low-mineralized samples: Mg-Ca-$HCO_3$, high-mineralized samples: Na-$HCO_3$, PA: Pampeano aquifer, F-KA: fractured-karstic aquifer, SW: surface water). The study area piezometric map was obtained from Glok Galli et al. [37] and the Del Azul Creek Basin (DACB) limit was elaborated by the Instituto de Hidrología de Llanuras 'Dr. Eduardo J. Usunoff' (UNCPBA-CIC-Azul Municipality). The black dashed box shows the area represented in Figure 2.

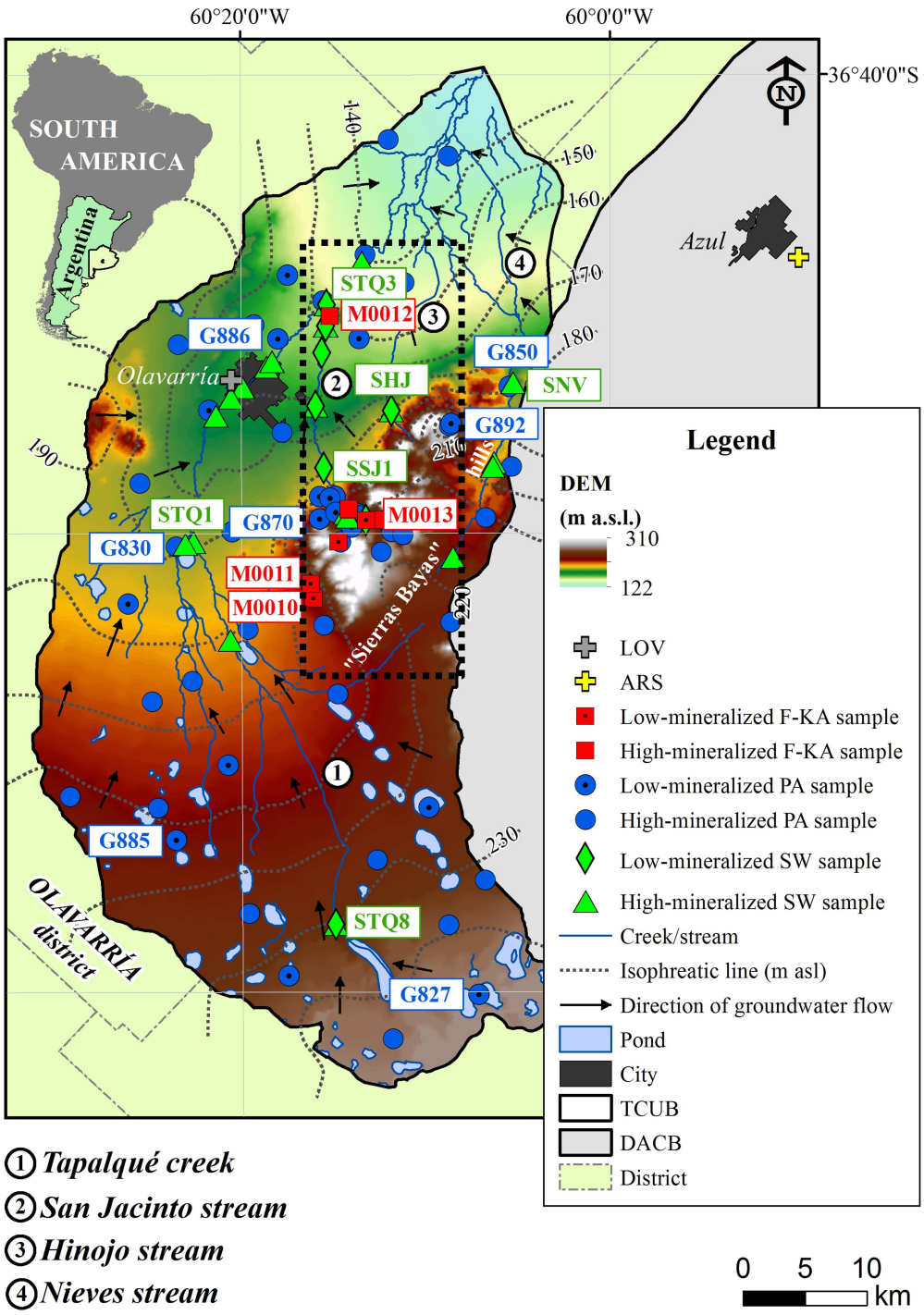


While these previous studies have provided an understanding of the connectivity between SW and the PA, the interactions between the PA and other aquifers in the area remained little understood. This study hypothesises that there is a close relationship between the hydrological components of catchments areas located to the southeast of the Pampa plain in Argentina: the detritic aquifers and F-KAs and SWs. The possibility of exploiting water not only from the PA but also from the F-KAs is a topic of interest for this zone. Therefore, the aim of this work is to analyze the interaction and potential contribution from F-KAs to the PA as the dominant detritic aquifer in the Olavarría region, through the joint application of hydrochemical and isotopic ($\delta^2$H , $\delta^{18}$O, $\delta^{13}$C-TDIC, $\delta^{18}$O-TDIC, $^{87}$Sr/$^{86}$Sr) tools. The use of $\delta^{13}$C-TDIC, $\delta^{18}$O-TDIC and $^{87}$Sr/$^{86}$Sr considers a novel aspect in the area, this work being of potential interest to local resource managers.

## 2. Description of the study area

The TCUB is located in the centre of the Buenos Aires province in Argentina, covering the northwestern part of the Olavarría Mountain Ranges, in this area known as Sierras Bayas, and the northern sector of the inter-mountain plain [39]. It is mostly situated in the Olavarría district, one of the main mining sites of the country, and occupies an area of approximately 2100 km$^2$. It is characterised by a low regional topographic gradient (0.3%) and altitudes up to 310 meters above sea level (m a.s.l.). The prevailing geomorphological setting is the plain, with elevations of up to 120 m a.s.l., which exceptionally reach 250 m a.s.l. in the southern sector (Figure 1). The area has a humid temperate climate, Cfa in the Köppen-Geiger classification [40], with a mean value of annual accumulated precipitation of around 900 mm (1949–2015) [37,38].

The TMS is a mountain range consisting of blocks lined up according to three Tertiary fault systems trending NW–SE, NE–SW and E–W, producing horst and graben structures and with strata dipping gently to the SW. In the study area, those blocks are formed by Paleoproterozoic crystalline basement rocks that conform the Buenos Aires Complex (2.26 Ga.) [29,41,42], and the overlaying Neoproterozoic sedimentary rocks

of the Sierras Bayas Group [43,44] (Figure 2). These constitute the F-KAs of the area. The igneous-metamorphic Buenos Aires Complex [45] mainly consists of granitoids, orthogneisses and migmatites. The Sierras Bayas Group consists of dolomite and limestone rocks. The Loma Negra (limestones) Formation (~ 40 m; ~ 543–560 Ma) [46] is its uppermost depositional sequence.

**Figure 2.** Geological map and 3-D real conceptual model of the area included in the black dashed box shown in Figure 1. The 3-D section was modified from Silva Busso and Amato [53] (P and Pp sediments: Pampeano and Postpampeano sedimients, m a.s.l.: meters above sea level, m b.g.s.: meters below ground surface, W-1 and W-2: well 1 and well 2, N/D: not determined). The four steps in which the hydrochemical modelling was performed are also displayed.

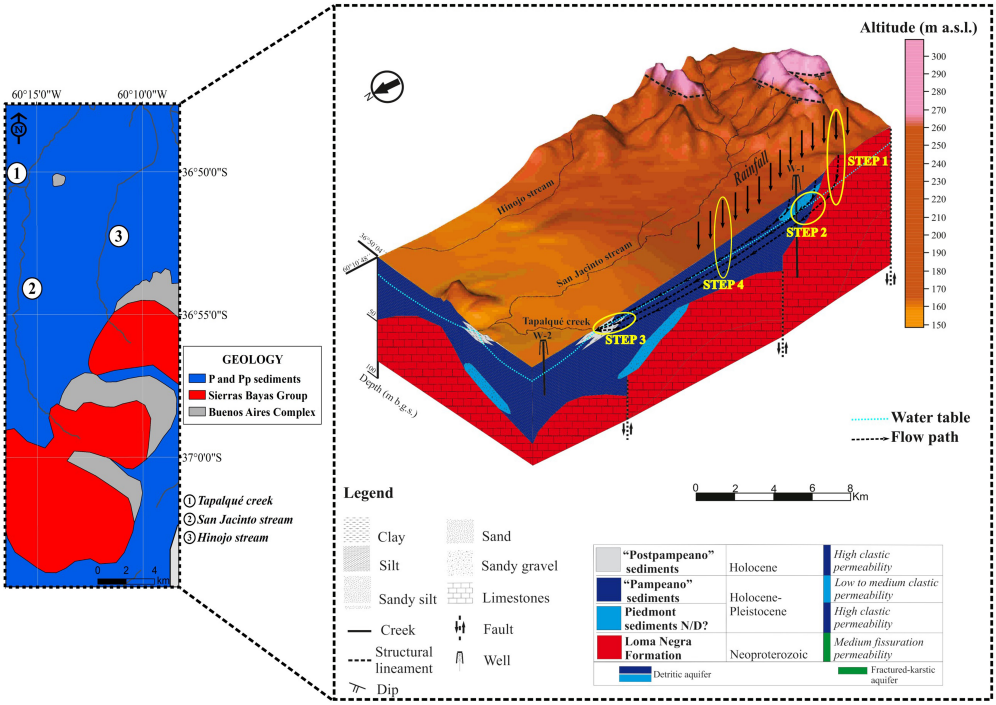


Quaternary sediments with primary permeability, called Pampeano (Pleistocene–Holocene) and Postpampeano (Holocene) [39], overlay the Buenos Aires Complex and the Sierras Bayas Group (Figure 2). These sediments are hydraulically linked, constituting the detritic aquifer unit of the zone, the PA. This sequence consists of silt and sandy silts with clay (at the top) and gravel and sand (at the bottom) intercalations. Layers of tosca or powdered $CaCO_3$ (calcrete) and volcanic ash are sporadically present. The main mineralogical composition is quartz, plagioclase and potassium feldspar (K-feldspar) with variable amounts of amorphous silica and minor proportions of micas and opaque minerals. Montmorillonite and illite are dominant in the clay size fraction. The presence of intra-sedimentary gypsum, halite, calcite and dolomite has also been described [47–51]. Precipitation is the main source of recharge for the PA [31,35,37,38]. Regional groundwater flow originates in the southern sector and receives local groundwater contributions from the northwestern and northeastern areas, where the mountain range outcrops are located. Natural discharge occurs through the hydrographic network into the Tapalqué creek and its tributaries, the San Jacinto, Hinojo and Nieves streams (all of which are gaining streams); in turn, anthropic output are production wells [31,35,37] (see piezometric map in Figure 1).

Auge [52] pointed out that 'the Pampeano aquifer upper section contains the water table, while the confinement degree increases with depth, until it becomes semi-confined below 40 or 50 m'. Silva Busso and Amato [53] propose that the F-KAs are probably unconfined in the outcropping sections of the mountain ranges and semi-unconfined to confined where the Pampeano sediments cover the piedmont zone.

## 3. Materials and methods

Samples of rainfall from the Olavarría (LOV) station (36°53'19.1'' S, 60°20'33.9'' W; 163 m a.s.l.), groundwater from wells of the PA and from springs and wells developed/drilled in granitic and limestone rocks of the F-KAs, and SW from streams and quarry reservoirs were analysed for chemical and isotope analyses ($\delta^2$H, $\delta^{18}$O, $\delta^{13}$C-TDIC, $\delta^{18}$O-TDIC, $^{87}$Sr/$^{86}$Sr) (Figure 1). For the hydrochemical characterisation, 17 rainwater samples, 95 PA samples, 11 F-KA samples and 108 SW samples were analysed. $\delta^2$H and $\delta^{18}$O were analysed in 19 rainfall samples, 50 PA samples, 6 F-KA samples and 47 SW samples. $\delta^{13}$C-TDIC and $\delta^{18}$O-TDIC were determined in 6 PA samples, 4 F-KA samples and 5 SW samples. Lastly, $^{87}$Sr/$^{86}$Sr ratios were measured in only three samples as a preliminary survey, one from the PA and two from the F-KA (spring waters in granitic rocks and in the limestone formation). Most of the samples were taken in the period from 2015 to 2019, but some previously unpublished hydrochemical data of SW samples collected since 1993 and F-KA and PA samples taken since 2002 were used as complementary information. A statistical test of the differences in the chemical composition among sampling dates could not be performed because only few duplicate sampling points of the PA were available. However, an exploratory observation based on a Schoeller diagram for sample G827 (Figure 1), the well with the highest number of analyses (from 2009 to 2018), allowed assuming no significant variability (Supplementary Figure 1).

Temperature, pH and electrical conductivity (EC) were determined *in situ* at each point using a portable multi-parameter instrument (HACH Pocket Pro Multi2). Measurement errors were ±0.5 °C for temperature, ±0.01 for pH and ±1% for EC. Probes were calibrated before each

sampling campaign. Chemical and water isotope analyses were performed at the Chemistry Laboratory of the National University of the Center of Buenos Aires Province, and the Hydrogeochemistry and Isotope Hydrology Laboratory of the University of Mar del Plata, Argentina, respectively.

Major ion concentrations were determined by standard methods detailed in APHA-AWWA-WPCF [54]: Mohr method for $Cl^-$, turbidimetry for $SO_4^{2-}$, complexometric titrations with EDTA for $Ca^{2+}$ and $Mg^{2+}$, flame spectrometry for $Na^+$ and $K^+$, and potentiometric titration for \hbox{HC}\hbox{O}_3^--\hbox{C}\hbox{O}_3^{2-}. Analytical uncertainties were 1.7% for $Cl^-$, 1.9% for $SO_4^{2-}$, 0.8% for $Ca^{2+}$ and $Mg^{2+}$, 4% for $Na^+$ and 2.3% for $K^+$. The analytical error for $HCO_3^-$ and $CO_3^{2-}$ is in the order of an average value of 5%. PHREEQC software [55] was used for the calculation of the gypsum, calcite and dolomite saturation indices ($SI_{gyp}$, $SI_{cal}$ and $SI_{dol}$, respectively).

Following the main hypothesis and the conceptual model, an inverse geochemical modelling was conducted using NETPATH [56] to assess the likelihood of a flow pathway that would connect F-KA to PA and ultimately to SW (Table 1). The first step (1a and b) was to consider that rainwater infiltration results into groundwater at the recharge area. The average chemical composition of the 17 LOV rainfall samples was used as initial composition, and the final was a representative sample of the F-KA (M0013; Figure 1). The second step (2) was to consider the evolution of F-KA water transferred to PA (sample G870; Figure 1) at the recharge zone. In the following model, groundwater from a mix between rainwater and PA (3a) or from PA (3b) is considered as initial water discharging into gaining streams (samples SSJ1 and STQ1, respectively; Figure 1), explaining the chemical evolution at the discharge area. The final step (4) was developed in order to check the hypothesis of direct recharge of the PA by rainwater infiltration (Figure 2).

**Table 1.** NETPATH inverse models results for different steps in the flow-path. The mass balance was performed with the elements and ions: C, S, $Cl^-$, $Na^+$, $K^+$, $Ca^{2+}$ and $Mg^{2+}$ (mass transfers indicated in mol/L). See location samples in Figure 1.

| Initial sample/s | Final sample | Step | Albite | Biotite | $CO_2$(g) | Calcite | Dolomite | Exchange Ca/Na | Exchange Mg/Na | Gypsum | NaCl | Evap./Mixingrates |
|---|---|---|---|---|---|---|---|---|---|---|---|---|
| LOV | F-KA(M0013) | 1a | 0.429 | 0.133 | 3.689 | −3.248 | 4.280 | – | – | 0.067 | 1.194 | – |
| LOV | F-KA(M0013) | 1b | 0.396 | 0.025 | 0.670 | −0.784 | 1.042 | – | – | −0.042 | – | 3.393 |
| F-KA(M0013) | PA(G870) | 2 | – | – | −0.28 | −1.185 | 0.615 | −0.156 | −0.615 | 0.365 | 0.311 | – |
| LOV + PA(G870) | SW(SSJ1) | 3a | – | – | 1.500 | −0.888 | 2.361 | 0.670 | – | 0.013 | – | 0.820.18 |
| PA(G870) | SW(STQ1) | 3b | – | 0.180 | 1.639 | −2.764 | – | −2.118 | 3.867 | −0.027 | – | 1.330 |
| LOV | PA(G870) | 4 | – | 0.108 | 3.199 | −4.337 | 4.954 | – | 0.059 | 0.432 | 1.505 | – |

Note: Evap.: evaporation.

The reactant phases included in the models are: albite, biotite, $CO_{2(g)}$, calcite, dolomite, gypsum, halite and ionic exchange of $Na^{2+}$, $Ca^{2+}$ and $Mg^{2+}$ (mass transfers indicated in mol/L). These reactant processes were selected from the analyses of the chemical data: (1) a $CO_{2(g)}$ open system can be assumed from the unconfined condition of the PA upper section [52] and the F-KA in the outcropping sections of the hills area [53]; (2) the clay-size particles percentage in the sediments, which provokes higher exchange capacity [48]; (3) the abundance of $CaCO_3$ as calcrete in the PA sediments and as calcite in the limestones of the F-KA [46]; (4) the presence of gypsum and halite [49–51], and also plagioclase, opaque minerals and dolomite [47] in the cement composition of the geological units under study; and (5) the previous investigations conducted in the area [31–38].

The $\delta^2H$ and $\delta^{18}O$ analyses were performed by laser spectroscopy [57] using a LIWA-45EP analyzer from Los Gatos Research Inc. The results were expressed as $\delta$ values per mile (‰), defined as:

$$\delta = 1000\lpar {\hbox{R}_{\rm s}\ndash \hbox{R}_{\rm p}} \rpar /\hbox{R}_{\rm p}\perthousand \comma \;$$

where $\delta$ is the isotopic deviation in ‰, S is the sample, P is the international reference and R is the isotopic ratio ($^2H/^1H$ and $^{18}O/^{16}O$ in this case), in accordance with the Vienna Standard Mean Oceanic Water (V-SMOW) international standards [58]. The analytical uncertainties were ±0.8 ‰ for $\delta^2H$ and ±0.12 ‰ for $\delta^{18}O$. The local meteoric water line (LMWL) obtained by Dapeña et al. [59] was considered in this work, since there is currently no record of more than 3 years of isotopic composition in the LOV rainfall collector. This LMWL was obtained for a period extending from January 1998 to December 2007 by means of orthogonal regression analysis from precipitation monthly composite samples from the Azul rainfall station (ARS; 36°47′59.5″ S, 59°49′47.8″ W; 137 m a.s.l.) (Figure 1), which is included in the Global Network of Isotopes in Precipitation (GNIP) [60].

The $\delta^{13}C$-TDIC and $\delta^{18}O$-TDIC analyses were performed at the Central Services for Research of the University of Málaga, Spain, using a

GasBench-II headspace autosampler in line with a Delta V Advantage mass spectrometer (Thermo Scientifics, Bremen, Germany). Laboratory standards were calibrated against NIST Standard Reference Materials (NBS-19, NBS-18 and LSVEC). The analytical error was ±0.1 ‰. The $^{87}Sr/^{86}Sr$ isotopic ratios were analysed at the Geochronology and Isotope Geochemistry Unit at the Research Support Center of the University of Madrid, Spain, using a TIMS-Phoenix mass spectrometer. The Sr isotope standard is NBS 987 ($^{87}Sr/^{86}Sr$ = 0.710248 ± 0.000003, NBS 1982, National Bureau of Standards Certificate of Analysis Standard Reference Material 987). The analytical error was ±0.01%.

Sample information and the results of hydrogeochemical analyses, saturation indices calculations and isotopic analyses are shown in Supplementary Tables 1, 2 and 3, respectively.

## 4. Results and discussion

### 4.1. Hydrochemical characterisation

Rainwater in the TCBU is classified as Mg–Ca-$HCO_3$-Cl type (Supplementary Figure 2a). F-KA is mostly characterised by Mg–Ca-$HCO_3$ water type (Supplementary Figure 2b). PA shows Mg–Ca-$HCO_3$ waters in the recharge zone, but Na-$HCO_3$ waters predominate in the discharge area and to the east of the water divide with the Del Azul Creek Basin (DACB) (Supplementary Figure 2c). The distribution of these two types of waters generally coincides with that characteristic of SW samples (Figure 1 and Supplementary Figure 2d).

As could be expected in phreatic/unconfined aquifers and/or in areas where calcite equilibrium prevails, $HCO_3^-$ content remains quite constant throughout the study area. However, the cationic composition is less homogeneous (see Supplementary Table 1 and the $SI_{cal}$ in Supplementary Table 2).

Significant reactions take place after rainwater infiltration of Mg–Ca-$HCO_3$-Cl type, from the recharge areas toward the discharge zone. Low-mineralized chemical composition (Mg–Ca-$HCO_3$) of F-KA samples is expected from rainwater interaction with the Loma Negra Formation's limestones ($CaCO_3$) in an area where this aquifer is unconfined. The F-KA is covered by the Pampeano sediments in the piedmont zones [53] (Figure 2) and a more evolved chemical composition (Na-$HCO_3$) is observed from wells drilled in these fissured limestones, as well as in the spring present in granitic rocks.

The lack of correlation between TDIC and/or $SO_4^{2-}$ and $Ca^{2+}$ indicates that calcite and gypsum dissolution is not the main process controlling the $Ca^{2+}$ content of the F-KA (Figure 3a, b), PA (Figure 3a-i, b–i) and SW (Figure 3a-ii, b-ii) sampling points. On the other hand, a moderate correlation between TDIC and $Ca^{2+}$ + $Mg^{2+}$ denotes that dolomite dissolution occurs as a process that controls $Ca^{2+}$ and $Mg^{2+}$ content, mainly in the low-mineralized F-KA (Figure 3c), PA (Figure 3c-i) and SW (Figure 3c-ii) samples. This is corroborated by the undersaturated $SI_{gyp}$ values in the entire study area, while the $SI_{cal}$ and SIdol values are close to equilibrium and oversaturated (Supplementary Table 2). These dissolution processes have been described in comparable scenarios by Cartwright and Weaver [9], Hofmann and Cartwright [12] and Santoni et al. [16].

**Figure 3.** Plots of TDIC vs. $Ca^{2+}$, $SO_4^{2-}$ *vs.* $Ca^{2+}$ and TDIC *vs.* $Ca^{2+}$ + $Mg^{2+}$ for F-KA (a, b, c), PA (a-i, b-i, c-i) and SW (a-ii, b-ii, c-ii) samples.

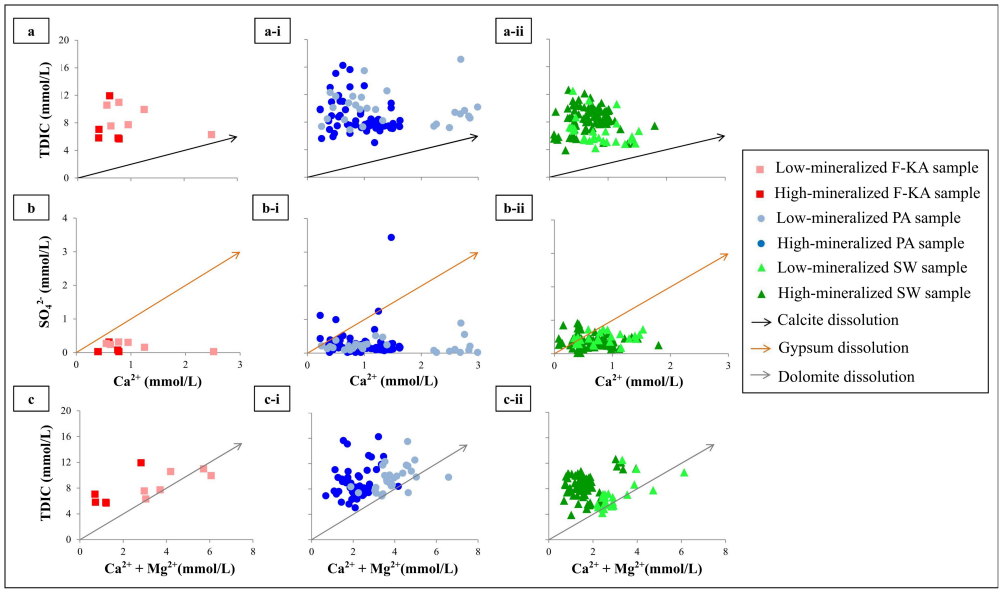


Molar Ca/Cl, Mg/Cl, Na/Cl and K/Cl ratios vs. $Cl^-$ (Figure 4a–d) indicate the importance of rock weathering, cationic exchange and evaporation on TCUB waters. Low levels of evaporation occur during direct recharge in the low-mineralized PA waters, whereas this process is significant in the high-mineralized PA and SW samples. The use of ionic ratios for inferring the occurrence of these types of processes was reported in previous works [9,12].

**Figure 4.** Molar a. Ca/Cl, b. Mg/Cl, c. Na/Cl and d. K/Cl *vs.* $Cl^-$ for F-KA (a-i, b-i, c-i, d-i), PA (a-ii, b-ii, c-ii, d-ii) and SW (a-iii, b-iii, c-iii, d-iii) samples.

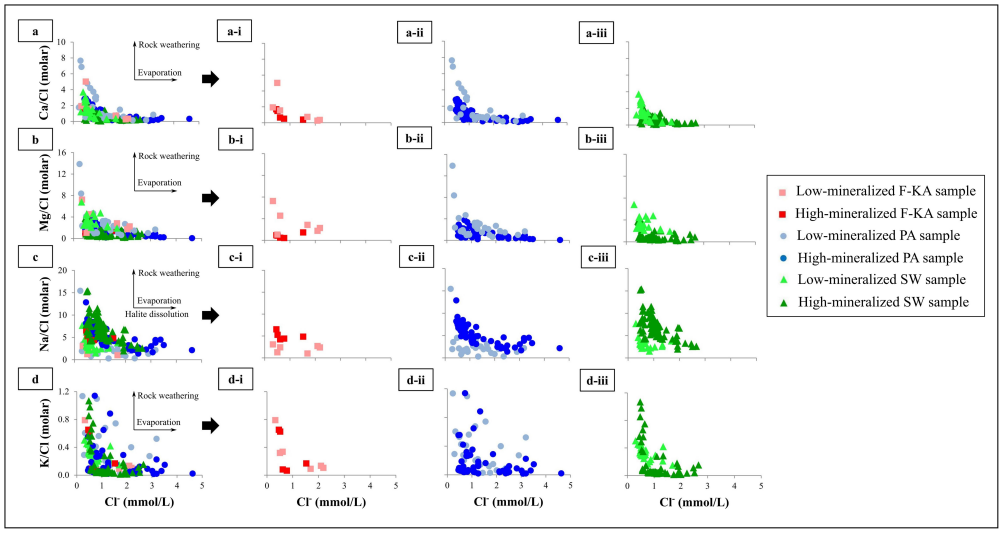


The relatively high Ca/Cl and Mg/Cl ratios of the low-mineralized F-KA (Figure 4a-i, b-i), PA (Figure 4a-ii, b-ii) and SW (Figure 4a-iii, b-iii) samples are explained by the dolomite (and gypsum) dissolution. Some of these samples have more $Ca^{2+}$ than $SO_4^{2-}$ (Figure 3b, b-i, b-ii) and $Ca^{2+} + Mg^{2+}$ than TDIC (Figure 3c, c-i, c-ii). Therefore, another main source of $Ca^{2+}$ and $Mg^{2+}$ may be the weathering of silicates, such as anorthite and mafic minerals (e.g. biotite or pyroxenes), respectively. Likewise, the lower Na/Cl ratio of these sampling points (Figure 4c-i, c-ii, c-iii) is similar to those observed in precipitation (between 0.02 and 1.12), when evaporation processes take place during infiltration [9,12,16].

The high-mineralized samples of F-KA and some of the PA and SW sampling points have more $Ca^{2+}$ than $SO_4^{2-}$ (Figure 3b, b-i, b-ii), which is mainly due to the dolomite dissolution, and may be also explained by the anorthite dissolution process. Conversely, the excess of $SO_4^{2-}$ with respect to $Ca^{2+}$ in some of these PA and SW samples (Figure 3b-i, b-ii) could be due to cationic exchange and the geochemical limitations for $Ca^{2+}$ concentrations (calcite precipitation). This ionic exchange reaction explains the higher Na/Cl ratios (Figure 4c-i, c-ii, c-iii) of these samples, which could also be controlled by the albite dissolution process in the F-KA. The low Na/Cl ratios observed in the high-mineralized PA and SW samples may be a consequence of the halite dissolution and concentration by evaporation. Finally, the high K/Cl ratios of some low- and high-mineralized F-KA (Figure 4d-i), PA (Figure 4d-ii) and SW (Figure 4d-iii) samples may be due to the weathering of K-feldspar (microcline) and/or mafic minerals such as biotite [9,12,16].

## 4.2. Hydrochemical modelling

The obtained inverse models validate the plausibility of the hydrochemical observations along a flow-path in three main steps, in which rainwater infiltrates into the F-KA and flows towards the PA, ultimately discharging into the SW. For step 1, the obtained results indicate as main processes: dissolution of albite, biotite and dolomite, the last inducing calcite precipitation, and halite dissolution (assuming this mineral presence in small amounts in the fractures of the F-KA; model 1a) or concentration by evaporation (model 1b) explaining the $Cl^-$ increase in the last two processes. Chemical changes in the water transfer from F-KA to PA (step 2) are due to the typical processes in the PA [50,61]: dolomite dissolution with calcite precipitation, cationic exchange and small amounts of halite and gypsum dissolution (Table 1).

Some streams have an intermediate $Cl^-$ content (Supplementary Table 1), suggesting mixing between groundwater discharge and surface runoff. Using $Cl^-$ for the mixing calculation (step 3a), a mixture of 82% of precipitation runoff expressed by the LOV average composition and 18% of groundwater was determined as components of a first order stream (San Jacinto stream). Dolomite dissolution with calcite precipitation, cationic exchange and gypsum dissolution are the reactions occurring during mixing. The composition of the Tapalqué creek shows higher salinity (Supplementary Table 1). This may be the result of the discharge of the PA plus an evaporation process and the characteristic reactions mentioned above: calcite precipitation and cationic exchange (step 3b). Finally, the large amount of calcite precipitation and dolomite dissolution obtained as result in the step 4 (LOV-PA hypothetical flow-line) is considered unlikely (Table 1). This reinforces the proposed conceptual model, in which the PA is likely to be partly recharged by waters from the F-KA.

## 4.3. Isotopic characterisation

### 4.3.1. Hydrogen and oxygen isotope variations

Water stable isotope results from the precipitation LOV station (monthly and weighted average values), and PA, F-KA and SW samples were plotted on a conventional diagram $\delta^2H$ vs. $\delta^{18}O$, together with the PA and SW trendlines, the global meteoric water line (GMWL) [62] and the LMWL from the ARS rainfall station (along with its weighted water isotopic composition). This is given by the equation $\delta^2H$ ‰ = (8.16 ± 0.12) $\delta^{18}O$ + (13.20 ± 0.66) ‰ ($R^2$ = 0.98) [59]. All trendlines were obtained through orthogonal regression (Figure 5). For LOV rainwater samples, the weighted isotopic composition ranges from −55.9 to 2.5 ‰, with a mean value of −23.4 ‰ for $\delta^2H$, and from −8.78 to −1.50 ‰, with an average value of −4.74 ‰ for $\delta^{18}O$. For the ARS rainwater, monthly weighted average values vary between −53.0 and −9.0 ‰ for $\delta^2H$ with an average of −31.0 ‰, and between −8.00 and −3.10 ‰ with a mean value of −5.50 ‰ for $\delta^{18}O$. At this station, the deuterium excess (*d*) values exceeded 10 (*d* monthly average = 13 ‰) [59] (Supplementary Table 3), which is characteristic of air masses caused by recycled vapour [63].

**Figure 5.** Water stable isotope composition ($\delta^2H$ vs. $\delta^{18}O$) of rainwater (LOV and ARS stations), F-KA and PA and SW.

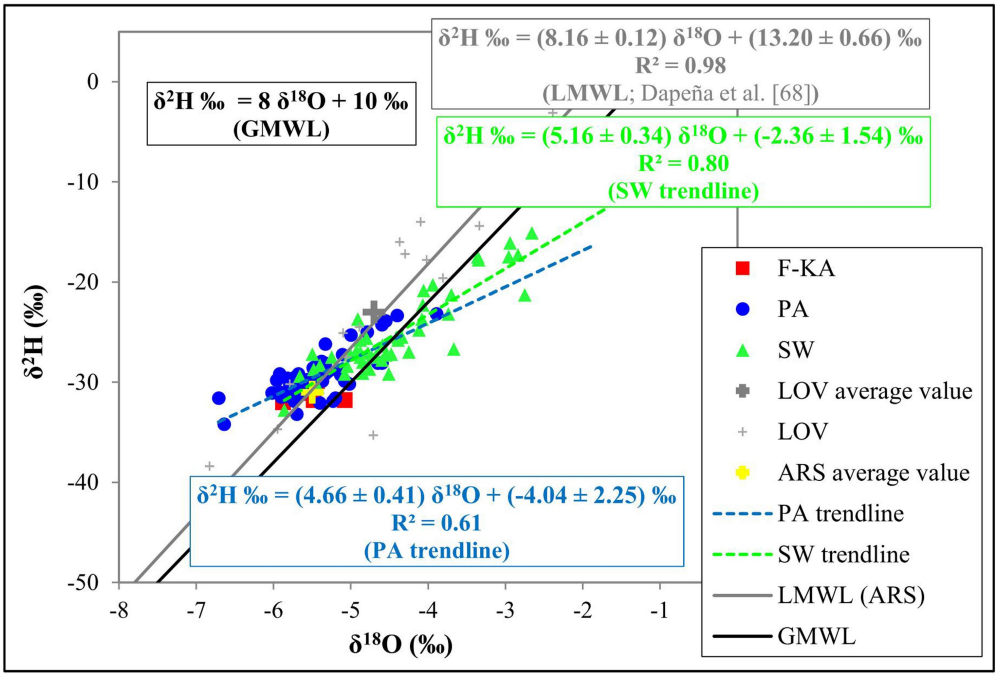


F-KA isotopic composition varies between −32.0 and −29.9 ‰, mean value −31.2 ‰ for $\delta^2$H, and from −5.88 to −5.08 ‰, mean −5.55 ‰ for $\delta^{18}$O. Samples from PA show $\delta^2$H and $\delta^{18}$O values ranging between −34.2 and −23.2 ‰ (mean value −29.4 ‰); and from −6.71 to −3.89 ‰ (mean −5.44 ‰), respectively. More enriched water infiltrated toward the plain zone, including some evaporation during infiltration (PA trendline equation: $\delta^2$H ‰ = (4.66 ± 0.41) $\delta^{18}$O + (−4.04 ± 2.25) ‰, $R^2$ = 0.61), which was inferred from the major ion geochemistry analysis. Likewise, the *d* values >10 of the ARS indicate a distinctive characteristic of rainwater in the area that is reflected in the F-KA (*d* average value 13.2 ‰) and PA (*d* average 14.2 ‰) waters (Supplementary Table 3).

Values of SW samples range from −32.8 to −15.1 ‰ (mean −25.3 ‰) for $\delta^2$H, and between −5.86 and −2.66 ‰ (mean −4.44 ‰) for $\delta^{18}$O. This isotopic composition is similar to that of the PA, suggesting the domain of the PA discharge into flow of the SW bodies. SW sampling points plot along a trendline corresponding to the equation $\delta^2$H ‰ = (5.16 ± 0.34) $\delta^{18}$O + (−2.36 ± 1.54) ‰ ($R^2$ = 0.80), which can be attributed to evaporation effects. The occurrence of this process is reflected in the lower SW *d* average value of 10.2 ‰ [63] (Supplementary Table 3) with respect to the ARS rainwater samples. Likewise, SW samples show significant scattering with respect to their trendline (Figure 5), and, in addition, the expected correlative increase in the EC values of some samples is not observed. The isotope enrichment of SW indicates a higher surface runoff component during the spring season, when $\delta^{18}$O values in the order of −2.39 ‰ were determined at LOV rainfall station samples (Supplementary Table 3).

#### 4.3.2. Carbon and oxygen isotope variations in TDIC and strontium isotope ratio

$\delta^{13}$C-TDIC values for the PA groundwater (low-mineralized water samples G850, G870, 6885, G886 and G892 and high-mineralized water sample G830) vary between −10.7 and −8.5 ‰ (mean −9.7 ‰). $\delta^{13}$C values range from −9.8 to −6.9 ‰ (mean −8.0 ‰), and from −11.4 to −9.3 ‰ (mean −10.1 ‰) for F-KA (low-mineralized water samples M0010, M0011 and M0013 and high-mineralized water sample M0012) and SW (low-mineralized water samples STQ8, SSJ1 and SHJ and high-mineralized water samples STQ3 and SNV), respectively (Figure 1). Variations of $\delta^{18}$O-TDIC range between −7.8 and −7.4 ‰ (mean −7.6 ‰) for the PA, from −7.5 to −7.3 ‰ (mean −7.4 ‰) for the F-KA, and between −7.4 and −6.1 ‰ (mean −6.7 ‰) for the SW samples (Supplementary Table 3).

The $^{87}$Sr/$^{86}$Sr ratios determined in the study area are 0.706978 for the PA sample (G870), and 0.707072 (M0012) and 0.707113 (M0013) for spring samples taken from granitic and limestone aquifers, respectively (Figure 1). The Sr isotopic signature of these three samples (~ 0.707) allows corroborating, on the one hand, the contribution from carbonates (around 0.708) [64] to the water composition of samples M0013 and G870, which is evidencing an F-KA contribution to the detritic aquifer. Groundwater that has dissolved carbonate minerals is expected to have low $^{87}$Sr/$^{86}$Sr ratios and relatively high $\delta^{13}$C-TDIC values (Figures 6 and 7) [65–68]. On the other hand, although it is expected that plutonic rocks will have higher $^{87}$Sr/$^{86}$Sr ratios (>0.715) [64], the Sr isotope ratio of sample M0012 is due to albite containing the least radiogenic type of Sr [69].

**Figure 6.** $\delta^{13}$C-TDIC *vs.* TDIC graph for the F-KA, PA and SW sampling points (diss.: dissolution). Samples location is shown in Figure 1.

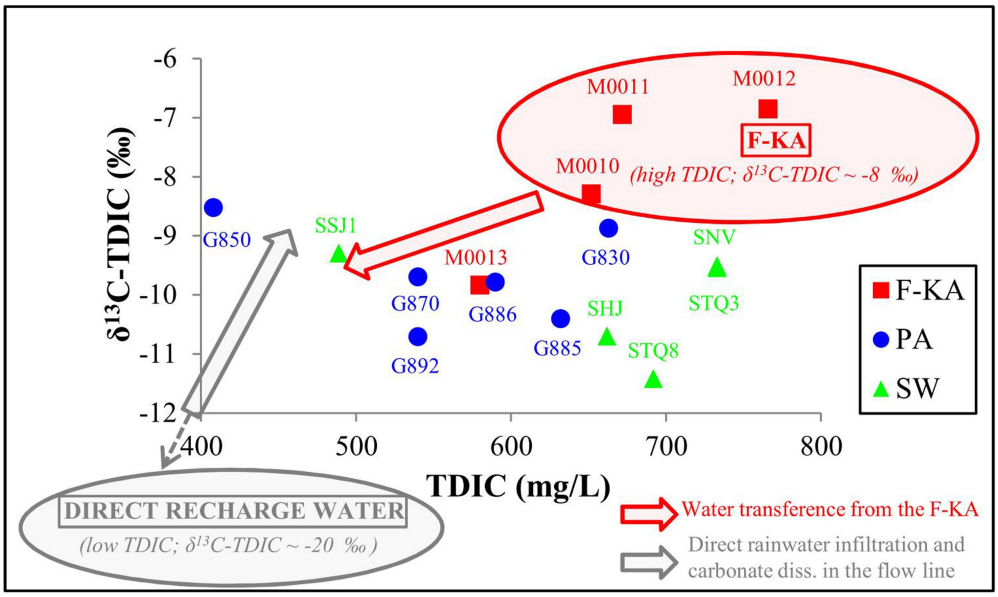


**Figure 7.** $\delta^{18}O$ *vs.* $\delta^{13}C$-TDIC graph for the F-KA, PA and SW sampling points. Samples location is shown in Figure 1.

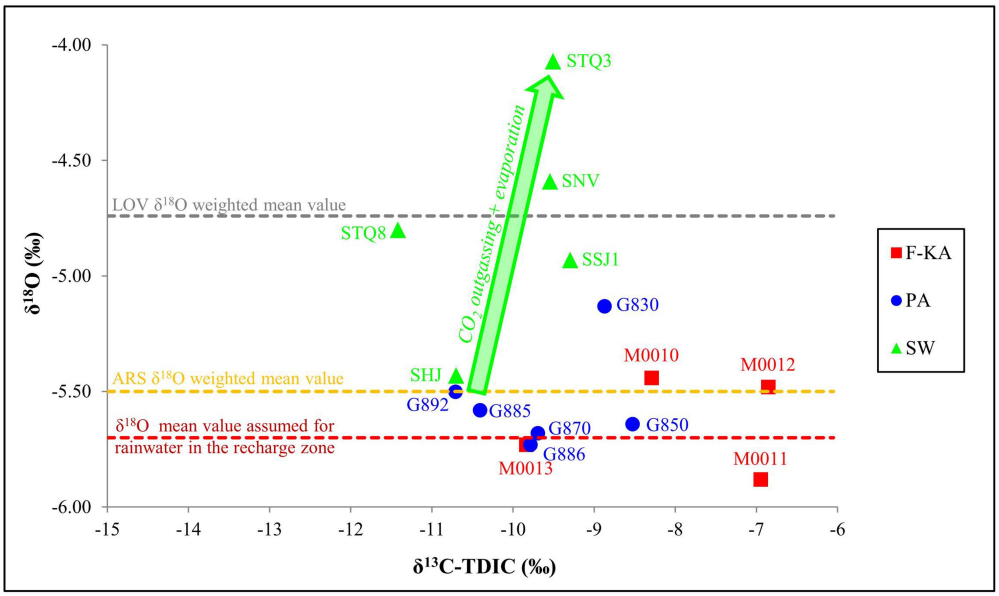


## 5. General discussion

The interaction between F-KA and PA can be hypothesised from their stratigraphic contacts and topographic positions. On the contrary, the usual consideration of the F-KA as an aquiclude constituting the hydrogeological basement tends to avoid or minimise this inter-relationship. Most of previous studies in the zone [31–37] considered that the PA is recharged by direct rain infiltration, ignoring the hydrological role of the F-KA. The application of chemical and isotope tracers has proven to be very useful to check the feasibility of aquifers connections in comparable scenarios [13–16].

Water stable isotopes support the hypothesis of lateral connectivity among aquifers. As can be seen in Figure 5, PA samples plot mostly between the LOV and ARS rainfall weighted average values, indicating that the main recharge is towards the hills area. The F-KA rocks outcrop in this mountain zone, corresponding to a more isotopically depleted recharge because of a slight altitude effect. The PA has more depleted water when it is in contact with the F-KA, but moving towards the plain area, its isotope composition is more depleted than that of the weighted average LOV rainfall station. In general, the ARS isotopic composition represents the end member of water recharged and flowing from the F-KA to the PA, while LOV composition represents the end member of water recharged directly into the PA. A similar application to identify mixing of different sources was performed by Négrel et al. [21].

Carbon isotopes and $^{87}Sr/^{86}Sr$ results have demonstrated to be useful tools for studying aquifer systems showing differences in their mineralogical composition [12]. This is the case of the TCUB, where the Buenos Aires Complex, Sierras Bayas Group and the Pampeano and Postpampeano Sediments are included. End member models to differentiate detritic to carbonate aquifers were successfully applied for layer interconnections by Brenot et al. [13].

Most of the TDIC in the study area occurs as $HCO_3^-$, since the pH values are under 8 in almost all water sampling points (Supplementary Table 1). Given the much higher TDIC concentrations in the PA, F-KA and SW samples (from ~ 400 to 800 mg/L) relative to LOV rainfall (average value 26.3 mg/L) (Supplementary Table 1), the increase in TDIC is likely to originate from water–rock interaction, more precisely, carbonate dissolution, which is higher in the F-KA.

In Figure 6, the F-KA is considered as an end member, following the same scheme used for water stable isotopes. It was assumed that: (1) the current atmospheric $CO_2$ ($CO_{2(atm)}$) has $\delta^{13}C$ ~ −8.4 ‰ [70], (2) the $\delta^{13}C$ of biogenic soil $CO_2$ ($CO_{2(soil)}$) ranges from −25.0 to −23.0 ‰ in soils hosting Calvin or $C_3$ vegetation and from −6.0 to −18.0 ‰ for the Hatch-Slack or $C_4$ crops existing in the area; and (3) the $\delta^{13}C$ for carbonate minerals is close to 0 ‰ [17,20]. The incorporation of $CO_2$ into the water takes place in an open system in the F-KA, increasing the TDIC content due to the dissolution of the geological materials present in the area. During this process, the $\delta^{13}C$-TDIC released into the water is a mixture between the isotopic signature of the $CO_{2(soil)}$ and that of carbonates. For open system conditions, final $^{13}C$-TDIC at calcite saturation is enriched by about 8 ‰ from the original $CO_{2(soil)}$ [17]. Considering the $\delta^{13}C$-TDIC value of around −8 ‰ for the end member F-KA, the contribution of $CO_{2(soil)}$ from $C_4$ plants is dominant [71].

The other end member is direct recharge water, having very low TDIC and $\delta^{13}C$-TDIC values in the range of about −20 ‰, considering mixing of $C_3$ (soy, grasslands) and $C_4$ crops (corn, wheats, sorghum) [71]. When this water reacts with the minerals in the PA (calcrete), TDIC increases and also $\delta^{13}C$-TDIC becomes more positive, as exemplified by sample G850 (Figure 6).

As seen in Figure 7, low-mineralized samples of F-KA and PA have similar $\delta^{18}O$ values, implying a similar recharge altitude and corroborating the hypothesis that PA waters come from F-KA in the TCUB recharge area. A $\delta^{18}O$ average value of ~ −5.70 ‰ can be assumed for rainwater in the recharge zone, considering a depletion of −0.5 ‰ per 100 m rise in altitude [17] and the 200 m difference (DEM in Figure 1) between the plain zone with weighted mean $\delta^{18}O$ of −4.74 ‰ (LOV station), and the mountain ranges. This is also reflected in the SHJ sample composition, given the water discharge from the PA into the stream [37,38]. The more enriched $^{18}O$ and $^{13}C$ contents of the other SW sampling points evidence the occurrence of $CO_2$ outgassing and the evaporation process. This is also supported by the more enriched $^{18}O$-TDIC ($\delta^{18}O$-TDIC: ~ −6.5 ‰) characteristic of these samples, which suggest evaporative loss [20] (Supplementary Table 3).

$^{87}Sr/^{86}Sr$ ratios are a very powerful tool as tracers for water–rock interactions and mixing processes in this type of granite–carbonate aquifers, as exemplified by Santoni et al. [16]. In this investigation, the few samples analysed prevent obtaining specific conclusions, but at least have been useful to identify a dominant carbonate dissolution source.

## 6. Conclusions

This multi-tracer study confirms that waters from the PA and F-KAs and SW bodies are closely interacting in the TCUB. The importance of rainwater infiltration in the highlands of fractured-karstified rock outcrops into the recharge zone of the PA groundwater system and subsequent transfer to this detritic aquifer was demonstrated. TDIC, stable isotopes of water and carbon in TDIC allowed differentiating two main end members. Water in the PA which is transferred from the F-KA is characterised by high TDIC around 500–700 mg/L, more isotopically depleted water ($\delta^{18}O$ ~ −5.5 ‰) and high $\delta^{13}C$–TDIC (~ −10.0 ‰). The other end member is direct recharge water infiltrated into the PA with TDIC values ranging from 400 to 500 mg/L, slightly isotopically enriched ($\delta^{18}O$ = −4.8 ‰), and $\delta^{13}C$-TDIC in the range of $CO_{2(soil)}$ interacting with calcrete concretions (from ~ −20.0 to −9.0 ‰).

A thermodynamically based mass balance hydrochemical model explains the dominant flow pathway, which validated the occurring chemical processes: dolomite dissolution is the main process controlling the chemistry of the low-mineralized (Mg–Ca-$HCO_3$) waters; while the high-mineralized (Na-$HCO_3$) waters are strongly influenced by ion-exchange reactions with adsorbed $Ca^{2+}$ and $Mg^{2+}$ and by evaporation. Calcite, gypsum, halite and silicate mineral dissolution are minor processes that control water chemical content. Regarding the TDIC content throughout the study area, this originates from varying degrees of carbonate dissolution and also from soil respiration ($CO_2$). These models are also consistent with the water stable isotope values during the evolution from rain infiltration (depleted values because of the altitude effect) to groundwater discharge into the streams (enrichment by evaporation).

Considering the F-KA and direct recharge water as end members, the interconnection of F-KA and PA aquifers is thus demonstrated, and a tool for determining the major inputs to the PA was obtained. These conclusions are of importance in terms of the water resources management in the study area, but can also be extrapolated to other zones where F-KAs and detritic aquifers are in contact.

Supplementary_material.doc


## Acknowledgments

This article is also a contribution to the Research Group of the 'Junta de Andalucía' (Hydrogeology Group, RNM-308). Authors~~We~~ are also thankful to Tec. G.V. Bernava and Prof. V. Colasurdo, who performed the chemical analyses. We recognise to anonymous reviewers, who largely contributed to the improvement of the manuscript.


## Disclosure statement

No potential conflict of interest was reported by the author(s).


## ORCID

*Melisa Glok-Galli* http://orcid.org/0000-0001-5470-8002


## References


1 **Scesi L, Gattinoni P.** Water circulation in rocks. Milano, Italy: Springer Science and Business Media; 2009.**[Q5]**

2 **Singhal BBS, Gupta RP.** Applied hydrogeology of fractured rocks. 2nd ed. Dordrecht, Netherlands: Springer Science and Business Media; 2010. **[Q6]**

3 **Dietrich P, Helmig R, Sauter M, et al.** Flow and transport in fractured porous media. Berlin, Germany: Springer Science & Business Media; 2005.**[Q7]**

4 **Pulido Bosch A.** Nociones de hidrogeología para ambientólogos. Almería: Editorial Universidad de Almería; 2014. Hidrogeología específica; p. 422–495. Spanish.

5 **Dreybrodt W.** Processes in karst systems. Heidelberg: Springer; 1988. (Springer Series in Physical Environment).

6 **Bakalowicz M.** Karst groundwater: a challenge for new resources. Hydrogeol J. 2005;13(1):148–160.

7 **Ford DC, Williams PW.** Karst hydrogeology and geomorphology. Chichester: Wiley; 2007.

8 **Appelo CAJ, Postma D.** Geochemistry, groundwater and pollution. Rotterdam: AA Balkema; 1993.

9 **Cartwright I, Weaver TR.** Hydrogeochemistry of the Goulburn Valley region of the Murray Basin, Australia: implications for flow paths and resource vulnerability. Hydrogeol J. 2005;13(5–6):752–770.

10 **Wang Y, Guo Q, Su C, et al.** Strontium isotope characterization and major ion geochemistry of karst water flow, Shentou, northern China. J Hydrol. 2006;328:592–603.

11 **Négrel P, Millot R, Guerrot C, et al.** Heterogeneities and interconnections in groundwaters: coupled B, Li and stable-isotope variations in a large aquifer system (Eocene Sand aquifer, Southwestern France). Chem Geol. 2012;296:83–95.

12 **Hofmann H, Cartwright I.** Using hydrogeochemistry to understand inter-aquifer mixing in the on-shore part of the Gippsland Basin, southeast Australia. Appl Geochem. 2013;33:84–103.

13 **Brenot A, Négrel P, Petelet-Giraud E, et al.** Insights from the salinity origins and interconnections of aquifers in a regional scale sedimentary aquifer system (Adour-Garonne district, SW France): contributions of $\delta^{34}S$ and $\delta^{18}O$ from dissolved sulfates and the $^{87}Sr/^{86}Sr$ ratio. Appl Geochem. 2015;53:27–41.

14 **Duvert C, Raiber M, Owen DD, et al.** Hydrochemical processes in a shallow coal seam gas aquifer and its overlying stream–alluvial system: implications for recharge and inter-aquifer connectivity. Appl Geochem. 2015;61:146–159.

15 **Owen DD, Raiber M, Cox ME.** Relationships between major ions in coal seam gas groundwaters: examples from the Surat and Clarence-Moreton basins. Int J Coal Geol. 2015;137:77–91.

16 **Santoni S, Huneau F, Garel E, et al.** Strontium isotopes as tracers of water–rocks interactions, mixing processes and residence time indicator of groundwater within the granite–carbonate coastal aquifer of Bonifacio (Corsica, France). Sci Total Environ. 2016;573:233–246.

17 **Clark ID, Fritz P.** Environmental isotopes in hydrogeology. Boca Raton (FL): CRC; 1997.

18 **Kendall C, McDonnell JJ**, editors. Isotope tracers in catchment hydrology. Amsterdam: Elsevier Science B.V.; 1998.

19 **Glok-Galli M, Damons ME, Siwawa S, et al.** Stable isotope hydrology in fractured and detritic aquifers at both sides of the south Atlantic Ocean: Mar del Plata (Argentina) and the Rawsonville and Sandspruit river catchment areas (South Africa). J South Am Earth Sci. 2017;73C:119–129.

20 **Mook G**, editor. Isótopos ambientales en el ciclo hidrológico. Publications of "Instituto Geológico y Minero de España", Guides and Manuals Series, Number 1. Madrid, Spain: IGME; 2002. Spanish.

21 **Négrel P, Casanova J, Aranyossy JF.** Strontium isotope systematics used to decipher the origin of groundwaters sampled from granitoids: the Vienne Case (France). Chem Geol. 2001;177(3–4):287–308.

22 **Soler A, Canals A, Goldstein SL, et al.** Sulfur and strontium isotope composition of the Llobregat River (NE Spain): tracers of natural and anthropogenic chemicals in stream waters. Water Air Soil Pollut. 2002;136(1–4):207–224.

23 **Petelet-Giraud E, Negrel P, Casanova J.** Variability of $^{87}Sr/^{86}Sr$ in water draining granite revealed after a double correction for atmospheric and anthropogenic inputs. Hydrol Sci J. 2003;48(5):729–742.

24 **Clark ID.** Groundwater geochemistry and isotopes. Boca Raton/London/New York: CRC Press/Taylor & Francis; 2015.

25 **Wetten C, Damiani O.** Estudio hidrogeológico del Karst de Los Berros (Argentina) para abastecimiento industrial. Antecedentes. I Geology Symposium, Nerja Cave; 1999. Spanish.

26 **Aguilera EY, Carretero S, Rabassa J.** Pseudokarst and speleothems in the Chihuido granite, province of Mendoza, Argentina. In: **Rabassa J, Ollier C**, editors. Gondwana landscapes in Southern South America. Dordrecht: Springer; 2014. p. 503–515.

27 **Nágera JJ.** Historia Física de la Provincia de Buenos Aires, Volume I Tandilia. Humanities and Education Sciences Library. La Plata University, La Plata, Buenos Aires, Argentina. 1940;24:1–272. Spanish.

28 **Teruggi ME, Kilmurray JO.** Tandilia. In: Report "Geología de la provincia de Buenos Aires", 6° Argentine Geological Congress; 1975. p. 55–77.

29 **Teruggi ME, Kilmurray JO.** Sierras Septentrionales de la Provincia de Buenos Aires. In: Turner, J.C.M. (Ed.), Proc. 2° Argentine Regional Symposium. National Academy of Sciences of Córdoba, vol. 2. Córdoba, Argentina; 1980. p. 919–956. Spanish.

30 **Dalla Salda LH, Spalletti L, Poiré D, et al.** Tandilia. In: Aceñolaza FG, editor. Temas de la Geología Argentina 1. San Miguel de Tucumán: INSUGEO; 2006. p. 17–46. (Serie Correlación Geológica; 21). Spanish.

31 **Auge MP.** Abastecimiento de agua potable a la ciudad de Olavarría, provincia de Buenos Aires – Informe final. Consejo Federal de Inversiones, Municipalidad de Olavarría, Obras Sanitarias de la provincia de Buenos Aires; 1993. Spanish.

**32 Díaz O, Usunoff E, Colasurdo V, et al.** Estudio físico–químico–bacteriológico del arroyo Tapalqué en la ciudad de Olavarría e hidroquímica de las aguas subterráneas de la región. In: Proceedings of "IV Jornadas Geológicas y Geofísicas Bonaerenses, 2"; Junín; Buenos Aires; 1995. p. 285–289. Spanish.

**33 Díaz O, Colasurdo V, Usunoff E.** Inferencias hidrodinámicas a partir de datos hidroquímicos en la cuenca del arroyo Tapalqué. In: Proceedings of "I Congreso Nacional de Hidrogeología"; Bahía Blanca, Buenos Aires; 1997. p. 267–279. Spanish.

**34 Kruse E, Rojo A, Varela L.** Características Hidroquímicas Subterráneas de la Cuenca del Arroyo Tapalqué (Buenos Aires). In: Proceedings of XII Argentine Geological Congress, II Hydrocarbon Exploration Congress, Volume VI; Argentina; 1993. p. 208–215. Spanish.

**35 Varela LB.** Escurrimiento subterráneo en la cuenca del arroyo Tapalqué. In: Situación Ambiental de la Provincia de Buenos Aires. A. Recursos y rasgos naturales en la evaluación ambiental, año II, no. 11. Coordination: Dr. López HL and Dr. Tonni EP. Buenos Aires, Argentina: Comisión de Investigaciones Científicas; 1992. Spanish.

**36 Varela L, Deluchi M, Laurencena P, et al.** Particularidades del flujo subterráneo en la región inferior del arroyo Tapalquén (provincia de Buenos Aires). In: II Congreso Argentino de Hidrogeología (Santa Fe); INSUGEO; 1999. (Serie Correlación Geológica; 13). Spanish.

**37 Glok-Galli M, Martínez DE, Colasurdo V, et al.** Caracterización hidrogeoquímica e isotópica de la cuenca alta del arroyo Tapalqué, provincia de Buenos Aires. In: García RF, Mariño EE, editors. Calidad del Agua Subterránea [Groundwater Quality Workshop]. IX Congreso Argentino de Hidrogeología y VII Seminario Hispano-Latinoamericano Sobre Temas Actuales de la Hidrología Subterránea, San Fernando del Valle de Catamarca, Catamarca, Argentina Catamarca: Editorial Científica Universitaria; 2016. p. 272–279. Spanish.

**38 Glok-Galli M, Barredo Codesal SP, Martínez DE, et al.** Hydrogeochemical and isotopic characterization of the Tapalqué creek upper basin and its associated karst, Buenos Aires, Argentina. In: Moore K, White S, editors. Proceedings of the 17th International Congress of Speleology, Sydney 2017, Volume 2. Sydney, NSW, Australia: Australian Speleological Federation Inc. Sydney; 2017. p. 16–21.

**39 Frenguelli J.** Rasgos generales de la morfología y geología de la Provincia de Buenos Aires. La Plata, Buenos Aires, Argentina: Ministerio de Obras Publicas, Laboratorio de Ensayo de Materiales e Investigaciones Tecnológicas; 1950. Spanish.

**40 Kottek M, Grieser J, Beck C, et al.** World map of the Köppen-Geiger climate classification updated. Meteorol Z. 2006;15:259–263.

**41 Marchese HG, Di Paola EC.** Miogeosinclinal tandil. Rev Asoc Geol Arg. 1975;30(2):161–179.

**42 Marchese HG, Di Paola EC.** Reinterpretación estratigráfica de la Perforación Punta Mogotes N° 1, Provincia de Buenos Aires, República Argentina. Rev Asoc Geol Arg. 1975;30:44–52. Spanish.

**43 Dalla Salda LH, Iñiguez Rodríguez AM.** La Tinta, Precámbrico y Paleozoico de Buenos Aires. In: Proceedings 7 Argentine Geological Congress; Neuquén; 1979. p. 539–550. Spanish.

**44 Poiré DG, Spalletti LA.** La cubierta sedimentaria precámbrica/paleozoica inferior del Sistema de Tandilia. In: Geología y Recursos Minerales de la provincia de Buenos Aires. Report XVI Argentine Geological Congress; 2005. p. 51–68. Spanish.

**45 Pankhurst RJ, Ramos A, Linares E.** Antiquity of the Río de la Plata craton in Tandilia, southern Buenos Aires province, Argentina. J South Am Earth Sci. 2003;16:5–13.

**46 Poiré DG, Gaucher C.** Lithostratigraphy. Neoproterozoic Cambrian evolution of the Río de la Plata Palaeocontinent. In: Gaucher C, Sial AN, Halverson GP, et al., editors. Neoproterozoic–Cambrian tectonics, global change and evolution: a focus on southwestern Gondwana. Elsevier; 2009. p. 87–101. (Developments in Precambrian Geology; 16).

**47 Teruggi ME.** El mineral volcánico-piroclástico en la sedimentación cuaternaria argentina. Rev Asoc Geol Arg. 1954;IX(3):184–191. Spanish.

**48 Teruggi ME.** The nature and origin of Argentine Loess. J Sediment Petrol. 1957;27(3):322–332.

**49 Dangavs N, Blasi A.** Los depósitos de yeso intrasedimentario del arroyo El Siasgo, partidos de Monte y General Paz, provincia de Buenos Aires. Rev Asoc Geol Arg. 2002;57(3):315–327. Spanish.

**50 Quiroz Londoño OM, Martínez DE, Dapeña C, et al.** Hydrogeochemistry and isotope analyses used to determine groundwater recharge and flow in low-gradient catchments of the province of Buenos Aires, Argentina. Hydrogeol J. 2008;16(6):1113–1127.

**51 Vital M, Daval D, Clément A, et al.** Importance of accessory minerals for the control of water chemistry of the Pampean aquifer, province of Buenos Aires, Argentina. Catena. 2018;160:112–123.

**52 Auge M.** Regiones Hidrogeológicas: República Argentina y provincias de Buenos Aires, Mendoza, Santa Fe. E-Book. 2004. Spanish. http://tierra.rediris.es/hidrored/ebooks/miguel/RegionesHidrogeol.pdf.

**53 Silva Busso AA, Amato SD.** Aspectos hidrogeológicos de la región periserrana de Tandilia (Buenos Aires, Argentina). Bol Geol Miner. 2012;123(1):27–40. Spanish.

**54 APHA-AWWA-WPCF**. Métodos Normalizados para el Análisis de Aguas Potables y Residuales. Madrid, Spain: Ediciones Díaz de Santos S.A.; 1992. Spanish.

**55 Parkhurst DL, Appelo CA.** User's guide to PHREEQC, a computer program for speciation, reaction path, advective–transport, and inverse geochemical calculations. Reston (VA): US Geological Survey; 1999. (Water resources investigations report; 99-4259).

**56 Plummer LN, Prestemon EC, Parkhurst DL.** An interactive code (NETPATH) for modeling NET geochemical reactions along a flow PATH. Reston (VA): US Geological Survey; 1991. (Water resources investigations report; 91-4078).

**57 Lis G, Wassenaar LI, Hendry MJ.** High precision laser spectroscopy D/H and $^{18}O/^{16}O$ measurements of microliter natural water samples.

Anal Chem. 2008;80:287–293.

**58 Gonfiantini R.** Standards for stable isotope measurements in natural compounds. Nature. 1978;271:534–536.

**59 Dapeña C, Varni M, Panarello HO, et al.** Composición isotópica de la precipitación de la Estación Azul, provincia de Buenos Aires. Red Nacional de Colectores Argentina. In: Varni M, Entraigas i, Vives L, editors. Proceedings I International Congress of Plain Hydrology; 21–24/09/2010; Azul, Buenos Aires, Argentina. p. 386–393. Spanish.

**60 IAEA/WMO**. Global network for isotopes in precipitation. The GNIP Database. 2006. http://isohis.iaea.org.

**61 Martínez DE, Bocanegra EM.** Hydrochemistry and cationic exchange processes in the coastal aquifer of Mar del Plata, Argentina. Hydrogeol J. 2002;10(3):393–408.

**62 Craig H.** Standard for reporting concentrations of deuterium and oxygen-18 in natural waters. Science. 1961;133(3467):1833–1834.

**63 Jiménez-Martínez J, Custodio E.** El exceso de deuterio en la lluvia y en la recarga a los acuíferos en el área circum-mediterránea y en la costa mediterránea española. Bol Geol Miner. 2008;119(1):21–32. Spanish.

**64 Faure G.** Principles of isotope geology. 2nd ed. Hoboken (NJ): Wiley; 1986.

**65 Katz BG, Bullen TD.** The combined use of $^{87}Sr/^{86}Sr$ and carbon and water isotopes to study hydrochemical interaction between groundwater and lake water in mantled karst. Geochim Cosmochim Acta. 1996;60:5075–5087.

**66 Dogramaci SS, Herczeg AL.** Strontium and carbon isotope constraints on carbonate-solution interactions and inter-aquifer mixing in groundwaters of the semi-arid Murray Basin, Australia. J Hydrol. 2002;262:50–67.

**67 Faure G, Mensing TM.** Isotopes: Principles and applications. 3rd ed. Hoboken (NJ): Wiley & Sons; 2004.

**68 Cartwright I, Weaver TR, Petrides B.** Controls on $^{87}Sr/^{86}Sr$ ratios of groundwater in silicate-dominated aquifers: SE Murray Basin, Australia. Chem Geol. 2007;246:107–123.

**69 Bullen TD, Kendall C.** Tracing of weathering reactions and water flowpaths: a multi-isotope approach. In: **Kendall C, McDonnell JJ**, editors. Isotope tracers in catchment hydrology. Amsterdam: Elsevier; 1998. p. 611–646.

**70 Graven H, Allison CE, Etheridge DM, et al.** Compiled records of carbon isotopes in atmospheric $CO_2$ for historical simulations in CMIP6. Geosci Model Dev. 2017;10(12):4405–4417.

**71 Recavarren P.** La producción agropecuaria en Olavarría, Benito Juárez, Laprida y Gral. La Madrid: evolución y desafíos a futuro. 1st ed. Balcarce (Buenos Aires): INTA Ed.; 2016; Spanish.